ADVANCED HEALTHCARE MATERIALS
www.advhealthmat.de
www.MaterialsViews.com

In Vivo Host Response and Degradation of Copolymer Scaffolds Functionalized with Nanodiamonds and Bone Morphogenetic Protein 2

Salwa Suliman, Yang Sun, Torbjorn O. Pedersen, Ying Xue, Joachim Nickel, Thilo Waag, Anna Finne-Wistrand, Doris Steinmüller-Nethl, Anke Krueger, Daniela E. Costea, and Kamal Mustafa**

The aim is to evaluate the effect of modifying poly[(L-lactide)-co-(ε-caprolactone)] scaffolds (PLCL) with nanodiamonds (nDP) or with nDP+physisorbed BMP-2 (nDP+BMP-2) on in vivo host tissue response and degradation. The scaffolds are implanted subcutaneously in Balb/c mice and retrieved after 1, 8, and 27 weeks. Molecular weight analysis shows that modified scaffolds degrade faster than the unmodified. Gene analysis at week 1 shows highest expression of proinflammatory markers around nDP scaffolds; although the presence of inflammatory cells and foreign body giant cells is more prominent around the PLCL. Tissue regeneration markers are highly expressed in the nDP+BMP-2 scaffolds at week 8. A fibrous capsule is detectable by week 8, thinnest around nDP scaffolds and at week 27 thickest around PLCL scaffolds. mRNA levels of ALP, COL1α2, and ANGPT1 are significantly upregulating in the nDP+BMP-2 scaffolds at week 1 with ectopic bone seen at week 8. Even when almost 90% of the scaffold is degraded at week 27, nDP are observable at implantation areas without adverse effects. In conclusion, modifying PLCL scaffolds with nDP does not aggravate the host response and physisorbed BMP-2 delivery attenuates inflammation while lowering the dose of BMP-2 to a relatively safe and economical level.

1. Introduction

The limitations of current bone reconstruction techniques have led to increased interest in developing improved scaffolds for bone tissue engineering (BTE).[1] Currently, the "golden standard" clinical treatment of large bone defects include autografts or allografts.[2] Despite presenting successful healing, however, they carry drawbacks such as donor site morbidity, disease transmission, and immune rejections.[2] Synthetic polyesters have been used in the biomedical field and for producing scaffolds for BTE for decades.[3] Degradable copolymers such as poly[(L-lactide)-co-(ε-caprolactone)] (PLCL) produced by copolymerization have been recently exploited for BTE scaffolds due to their in vitro cytocompatibility,[4] osteogenic conductivity[5] in addition to tuneable mechanical and degradable properties.[6] Also, scaffolds produced by

Dr. S. Suliman, Dr. T. O. Pedersen, Dr. Y. Xue, Prof. K. Mustafa
Department of Clinical Dentistry
Center for Clinical Dental Research
University of Bergen
5009, Bergen, Norway
E-mail: salwa.suliman@iko.uib.no; kamal.mustafa@iko.uib.no
Dr. S. Suliman, Prof. D. E. Costea
Gade Laboratory for Pathology
Department of Clinical Medicine
University of Bergen
5020, Bergen, Norway
Dr. S. Suliman, Prof. D. E. Costea
Center for International Health
Department of Global Public Health and Primary Care
University of Bergen
5009, Bergen, Norway
Dr. Y. Sun, Assoc. Prof. A. Finne-Wistrand
Department of Fibre and Polymer Technology
KTH
Royal Institute of Technology
10044, Stockholm, Sweden
Dr. J. Nickel
Chair Tissue Engineering and Regenerative Medicine
University Hospital of Würzburg
97070, Würzburg, Germany
Dr. J. Nickel
Fraunhofer Institute for Interfacial Engineering and Biotechnology IGB
Translational Center "Regenerative Therapies for Oncology and Musculoskeletal Diseases"- Würzburg branch
D-97070, Würzburg, Germany
Dr. T. Waag, Prof. A. Krueger
Institute of Organic Chemistry
University of Würzburg
97074, Würzburg, Germany
Dr. D. Steinmüller-Nethl
DiaCoating GmbH
6020, Innsbruck, Austria
Prof. D. E. Costea
Department of Pathology
Hauekeland University Hospital
5020, Bergen, Norway

DOI: 10.1002/adhm.201500723

blending of poly(L-lactide) and polycaprolactone in different proportions significantly improved human stem cell attachment and growth when compared to homopolymers.[7] This blended polymer also exhibited characteristics favorable for bone regeneration in critical defects in ovine tibiae.[8]

It has been shown that the nanoscale architecture of bioengineered scaffold materials generates bioactive scaffolds, which can substitute for the native extracellular matrix and enable spatiotemporal release of relevant growth factors.[9] Carbon-derived nanodiamond particles (nDP) have gained wide attention in medical technology owing to their chemical stability and biocompatibility.[10] Recent reports have demonstrated that nDP with oxygen-containing terminal groups (mostly hydroxyl) enhance the hydrophilic properties of copolymer scaffolds, thus enhancing cellular responses and subsequent bone formation.[11] (PLCL) scaffolds and nDP have also shown to provide a promising delivery modality for low controlled amounts of osteogenic growth factors such as bone morphogenetic protein 2 (BMP-2).[12] Previously BMP-2 has been applied in supraphysiological doses for adequate bone regeneration.[13]

An implanted scaffold can act as a foreign material and the protein interactions at their surface are crucial for the nature of the host response toward it.[14] An implanted scaffold initiates a series of events similar to a foreign body reaction, starting with an acute inflammatory response and leading in some cases to a chronic inflammatory response and/or granulation tissue development, a foreign body reaction and fibrous capsule development. The chemical composition of the scaffold, its surface charge, porosity, topography, size, and shape affects the intensity and duration of each of the steps of this cascade.[15] Hence, functionalizing a scaffold with nDP may affect the host's tissue response. Titania[16] and tripolyphosphate nanoparticles[17] have been shown to improve the biocompatibility of poly(lactic-co-glycolic acid) scaffolds, while nondegradable nanoparticles made of silica have been shown to induce inflammation.[18] Inflammatory cell interactions significantly impact the biocompatibility and function of implanted scaffolds and can eventually cause their clinical failure[19] or success. For instance, local inflammation is required to initiate the process of tissue regeneration and its control is considered necessary to guide the normal regeneration of damaged tissues. However, both deficient and excessive inflammation can negatively affect the tissue regeneration process.[20] BMP-2 in high uncontrolled amounts have been used for bone regeneration clinically and occasionally been reported to cause unfavorable tissue effects, ranging from soft tissue edema, erythema, "unwanted" exaggerated inflammation, and immune response.[21] The control of inflammatory response to enhance bone regeneration has been extensively studied,[22] and it is widely believed that control of these responses leads to a diminished foreign body reaction and increased bone regeneration.[23]

To be used in regenerative medicine, a bioengineered scaffold must have good biocompatibility in the host tissue.[24] The degradation profile of a bioactive scaffold is essential, as it should degrade at a rate approximating the rate of tissue restoration while maintaining release of the appropriate concentration of the incorporated BMP-2. Also, neither the scaffold nor the by-products should be toxic.[1] The lack of adverse tissue responses to the scaffold delivering a growth factor in a host is one of the critical requirements of a tissue engineering construct in addition to supporting suitable cellular action and enabling molecular and mechanical support.[25] The degradation profile of pristine poly[(L-lactide)-co-(ε-caprolactone)] (PLCL) scaffolds has been previously reported, however only for up to 13 weeks in vivo.[26] The effect of nDP modification and BMP-2 physisorption on the degradation of these scaffolds has not been studied yet. Thus, the main objective of this work was to determine in vivo the effect of functionalizing PLCL scaffolds with nDP and nDP plus BMP-2 on degradation and on the inflammatory and healing response up to 27 weeks.

2. Materials and Methods

2.1. Scaffold Fabrication

The poly[(L-lactide)-co-(ε-caprolactone)] was synthesized by bulk-ring opening polymerization of the monomers L-lactide (Boehringer Ingelheim,Germany) and ε-caprolactone (Sigma-Aldrich, St Louis, MO, USA) as described earlier.[5] Briefly, L-lactide was purified by recrystallization in dried toluene for three times. The ε-caprolactone was dried through calcium hydride at room temperature overnight and distilled at 80 °C for purification. The components of monomers, initiator (ethylene glycol) and catalyst (stannous 2-ethylhexanoate) were loaded under inert environment. The reaction was performed under 110 °C for 72 h and precipitated three times in cold hexane and methanol to remove unreacted monomers.[5] The number average molecular weight (M_n) of the purified copolymer was ≈100 000 Da and molar mass dispersity ($Đ_m$) ≈1.3 determined by size exclusion chromatography (SEC) (Polymer Laboratories, U.K.). The copolymer was composed of 75 mol % L-lactide and 25 mol% ε – caprolactone, confirmed by proton nuclear magnetic resonance (^{1}H NMR) (Bruker Avance 400, Billerica, MA, USA). 3D porous scaffolds were prepared by the solvent-casting particulate leaching method described earlier.[5,6] The copolymer was dissolved in chloroform (1 g mL^{-1}) and mixed with sodium chloride particles by a weight ratio of 10:1 before being poured into molds. Scaffolds were punched out in a disc shape of (diameter ≈6 mm, thickness ≈1.3 mm). Salt particles were removed by soaking in deionized water and then scaffolds were vacuum dried and electron beam sterilized. Scaffold porosities before and after modification with nanodiamond alone or nanodiamond and BMP-2 were characterized using a micro-CT (SkyScan 1172, Kontich, Belgium) using 33 kV, 9 µm voxel, 0.4° rotation step and no filter. 3D reconstruction images were constructed with the software CT-Analyzer (v 1.13, Bruker).

2.2. Colloidal nDP Production and Scaffolds Modified with nDP Plus Physisorbed BMP-2 (nDP and nDP+BMP-2 Scaffolds)

Recombinant BMP-2 and colloidal nanodiamond particles were produced as previously described and the PLCL scaffolds modified as previously reported.[12] Briefly, BMP-2 expressed in Escherichia coli (*E. coli*), isolated from inclusion bodies,

renatured and purified. Each scaffold contained 1 µg of BMP-2. Acid purified detonation diamond (Gansu Lingyun Corp., Lanzhou, China) was subjected to attrition milling using a method previously described[27] achieving a narrow size distribution at ≈5 nm particle diameter (measured by dynamic light scattering in water) and very low agglomeration of the diamond particles. Scaffolds were modified with the nDP solution (2 wt%, i.e., 20 mg mL^{-1}) by a vacuum technique: 0.5 mL nDP solution and one scaffold were put in a glass beaker and perfused in vacuum (Oerlikon Leybold, TRIVAC D 65B). The vacuum chamber was evacuated down to the pressure where the nDP-water solution changes into vapor phase and the nDP burst into the scaffold surface. This cycle was repeated 10 times. After treatment, the nDP modified scaffolds were rinsed with distilled water and dried in vacuum for 8 h. To quantify the increase of the surface due to nDP retained in the scaffold, the Brunauer–Emmet–Teller (BET) isotherm was determined using N_2 at 77 K using an ASAP 2420 surface area and porosimetry system (Micromeritics). An increase of surface area after modification with nDP by factor 30 could be determined providing a large interactive area for subsequent physisorption with BMP-2. Quantitative measurement of the nDP in the scaffolds has been controlled for quality by induction furnace combustion for quantification of inorganic carbon amounts in solid materials.

BMP-2 was physisorbed onto unmodified PLCL scaffolds as follows: scaffolds were placed on a sterilized parafilm (M Barrier Film, Parafilm and 1 µg of BMP-2/ 50 µL phosphate buffered saline (PBS) was dropped as two equal portions onto the surface of the scaffold. The first aliquot was allowed to adsorb after which the second aliquot was added before the scaffold was used. Unmodified copolymer scaffolds are abbreviated as PLCL scaffold and copolymer scaffolds modified with nDP are abbreviated as nDP scaffold and scaffolds modified with nDP plus physisorbed with BMP-2 are abbreviated as nDP+BMP-2 scaffold.

2.3. Mouse Ectopic Subcutaneous Implantationn

Thirty female Balb/c mice (6–8 weeks) were anesthetized with Isoflurane (Isoba VetTM) (Schering Plough, Kenilworth, NJ, USA) before two incisions (1 cm) were made on their back. One incision was made between the upper limbs and another between the lower limbs. Four scaffolds were implanted into each mouse and the different groups (PLCL scaffolds, nDP scaffolds, and nDP+BMP-2 scaffolds) were distributed among all mice (n = 8 scaffolds per time point). Wounds were closed with Histoacryl tissue adhesive (B. Braun Surgical AS, Germany). Animals were sacrificed with CO_2 overdose at 1, 8, and 27 weeks after implantation. The samples were retrieved and stored in RNAlater (Invitrogen, Carlsbad, CA, USA) for quantitative real-time reverse transcribed polymerase chain reaction (RT-PCR), micro-CT, and histological analyses.

2.4. Copolymer Composition and Molecular Weight Analysis

The harvested samples after 1, 8, and 27 weeks were dissolved in chloroform. Number average molecular weights were recorded by SEC on a Verotech PL-GPC 50 (Polymer Laboratories, Varian Inc., MA, USA), equipped with a refractive index detector and two Polar-Gel-M organic GPC columns (300 × 7.5 mm) from Varian Inc. Samples were injected using a PL-AS RT auto sampler, using chloroform at a flow rate of 1mL min^{-1} as eluent. The system was calibrated against narrow polystyrene standards (Part No. PL2010-0301, range 162–371, 100 g mol^{-1}, Varian Inc.). The data were analyzed by Cirrus GPC software. An average of 2 samples is presented in the results. Molecular weight loss percentage was calculated using the following formula:

$$\text{Molecular weight loss} = \frac{\text{Initial } M_n \text{ of sample} - M_n \text{ of degraded sample} \times 100}{\text{Initial } M_n \text{ of sample}} \quad (1)$$

2.5. Gene Analysis by Customized RT^2 Profiler PCR Array

Total RNA was isolated from the in vivo samples after week 1 and week 8 using a Tissue RNA isolation kit (Maxwell, Promega, Madison, WI, USA) and reverse transcribed according to the manufacturer's instructions using the Rt^2 PCR array First Strand Kit (SABiosciences, Hilden, Germany). A customized Rt^2 Profiler PCR Array (SABiosciences) including selected inflammatory, osteogenic, and angiogenic probes was used and PCR was performed on a StepOne Plus real time PCR system (Applied Biosystems,Carlsbad, CA, USA) with Rt^2 Real-time SyBR Green/Rox PCR mix (Superarray Bioscience). The genes included in the assay are summarized in **Table 1**.

2.7. Descriptive Semiquantitative Histological Evaluation

Retrieved samples were fixed in 4% paraformaldehyde then decalcified over one week using 10% EDTA in 0.1*M* Tris buffer and 7.5 % Polyvinylpyrrolidone (Merck & Co, White House Station, NJ, USA) before embedding in paraffin. Sections of 3–4 µm were stained with hematoxylin/eosin (H&E) (Sigma, St Louis, MO, USA). Qualitative and semiquantitative histological evaluation was carried out to assess the tissues' response to the implanted scaffolds. Sections were evaluated blindly by two of the authors (S.S. and D.E.C, one is a pathologist) under a light microscope (Leica, Solms, Germany). The presence and quality of fibrous capsules and the type and amounts of cells were randomly evaluated in six fields of vision (magnification 400×) of the entire implant area of each section using a modified scoring system.[28] Histopathological examination of tissue specimens was limited to the tissue inside the scaffold and that in direct contact with it, evaluating the presence of different types of cells: those involved in early responses (neutrophils and plasma cells) and those involved in late or chronic responses (lymphocytes and foreign body giant cells). The grading for histological scoring is summarized in **Table 2**.

The histological sections were also visualized with an ultraresolution imaging system (Cytoviva 130, Auburn USA) consisting of a customized condenser (high resolution

Table 1. Functional grouping of the genes evaluated.

Gene	Full name
Inflammatory cytokines and chemokines	
CCL5	Chemokine (C–C motif) ligand 5-RANTES
IL 10	Interleukin 10
IL 4	Interleukin 4
IL 1a	Interleukin 1 alpha
IL 1b	Interleukin 1 beta – Catabolin
IL 6	Interleukin 6
TNFα	Tumor necrosis factor alpha
CSF1	Colony stimulating factor 1
CCL12	Chemokine (C-C motif) ligand 12
CXCR2	Chemokine (C-X-C motif) receptor 2
PECAM1	Platelet/endothelial cell adhesion molecule 1
MMP9	Matrix metallopeptidase 9
Osteogenic markers	
COL1α2	Collagen, type 1, alpha 2
COL2α1	Collagen, type 2, alpha 1
COL1α1	Collagen, type 1, alpha 1
ALP	Alkaline phosphatase
RUNX2	Runt-related transcription factor 2
BMP- 2	Bone morphogenetic protein 2
BMP-4	Bone morphogenetic protein 4
BMP-7	Bone morphogenetic protein 7
SOX9	Transcription factor sox 9
BMPR1A	Bone morphogenetic protein receptor 1A
BMPR2	Bone morphogenetic protein receptor 2
Angiogenic markers	
VWF	Von Willebrand factor
VEGFA	Vascular endothelial growth factor A
FGF2	Basic fibroblast growth factor
ANGPT1	Angiopoietin 1
ANGPT2	Angiopoietin 2
Endogenous references	
GAPDH	Glyceraldehyde 3-phosphate dehydrogenase
B2M	Beta-2 microglobulin
ACTβ	Actin beta

Table 2. Histological grading scale for tissue response.

Histological grading scales	Score
Grading scale for capsule thickness	
Not applicable	1
1–4 concentric layers of fibroblasts	2
5–9 concentric layers of fibroblasts	3
>30 concentric layers of fibroblasts	4
Grading scale for capsule quality	
Not applicable	1
Inflammatory cells with no fibers	2
Both fibers and inflammatory cells	3
Collagen fibers	4
Inflammatory cells (lymphocytes, neutrophils, plasma cells, giant cells)	
0–3	1
4–6	2
7–9	3
>10	4

illuminator) connected to a research grade optical microscope (Olumpus, BX41) and a powerful light source (EXF0120, Photonic Solution) equipped with a (100×) oil immersion objective. Images were captured with a cooled camera (model XLMCT, Dage-MTI, USA) and DageXponent software (v 1.3, Dage-MTI, USA).

2.8. Microcomputed Tomography

The amount of mineralized tissue (bone formation) within the scaffolds was examined using micro-CT (Skyscan 1172, Bruker) with ≈6–8 µm pixel size, 50 kV, aluminum 0.5 mm filter, and 0.4° rotation step. 3D reconstruction images were constructed with the software CT-Analyzer (v 1.13, Bruker).

2.9. Statistical Analysis

The average values were analyzed using SPSS Statistics 21.0 (IBM, Armonk, NY, US). RT-PCR data were analyzed using the web-based analysis software RT^2 Profiler PCR Array Data Analysis (v 3.5, Superarray Bioscience) and expressed as the mean with 95% confidence interval (CI). Other results were expressed as mean ± standard deviation (SD) and analyzed using One-way ANOVA followed by a multiple-comparison Tukey test. Differences between the means was considered statistically significant when $p < 0.05$.

2.10. Ethical Statement

All animal experiments were approved by the Norwegian Animal Research Authority and conducted in strict accordance with the European Convention for the Protection of Vertebrates used for Scientific Purposes (FOTS no. 20135042). All procedures were performed under isoflurane gas anesthesia, and all efforts were made to minimize suffering.

3. Results

3.1. Functionalizing Poly(LLA-co-CL) Scaffolds with nDP and nDP+BMP-2 Expedite their Degradation

Modifying the PLCL scaffolds with nDP or nDP+BMP-2 did not affect the porosity or pore distribution of the scaffolds

(Figure S1A,B, Supporting Information). The porosity of the different scaffolds was 88.5%, 86.8%, and 86.1% for PLCL, nDP, and nDP+BMP-2, respectively (Figure S1A, Supporting Information). After implantation, uneventful wound healing was observed at all time points and no notable macroscopic differences were observed in the implantation sites of the different scaffolds. No signs of systemic or neurological toxicity occurred during the observation period. The observations were based on lack of infection in surgical wound area, loss in weight (>10%), abnormal movement or immobility and ungroomed fur.

In vivo degradation of the different scaffolds was seen macroscopically and the profile was determined by the percentage loss in number average molecular weight of the polymer (**Figure 1**A). A dry scaffold representing each group from every time point is shown in (Figure 1C–F). Macroscopically they were seen to retain their general round shape and structure up to week 8. At week 27 the scaffolds became considerably thinner and translucent in central areas, which made them more susceptible to tearing. Molecular weight analysis showed that between week 1 and week 8 the rate of degradation was different for the different scaffolds. At week 1 more molecular weight loss was observed from the nDP and nDP+BMP-2 scaffolds than from the PLCL scaffolds. This trend was also seen at week 8, where the modified scaffolds lost more molecular weight than the PLCL scaffolds. At week 27 almost 90% of the polymer had degraded from all scaffold types. Images taken with ultrahigh resolution imaging (Cytoviva) microscopy showed that the nDP were still present in the implantation tissue area at week 27 (Figure 1G).

3.2. In Vivo Host Response and Expression of Inflammatory Markers

Gene analysis of the pro-inflammatory markers (cytokines) displayed a general upregulated expression at week 1 and relative downregulation at week 8 (**Figure 2**A). Early inflammatory chemokines (CCL5 and CCL12) were highly expressed in the modified group scaffolds compared to PLCL at week 1 and then significantly downregulated in all groups at week 8. IL6 showed significant upregulation for nDP at week 1. TNFα and IL10 showed a significant downregulation for all groups at week 8. However, markers of late/chronic inflammation or tissue healing

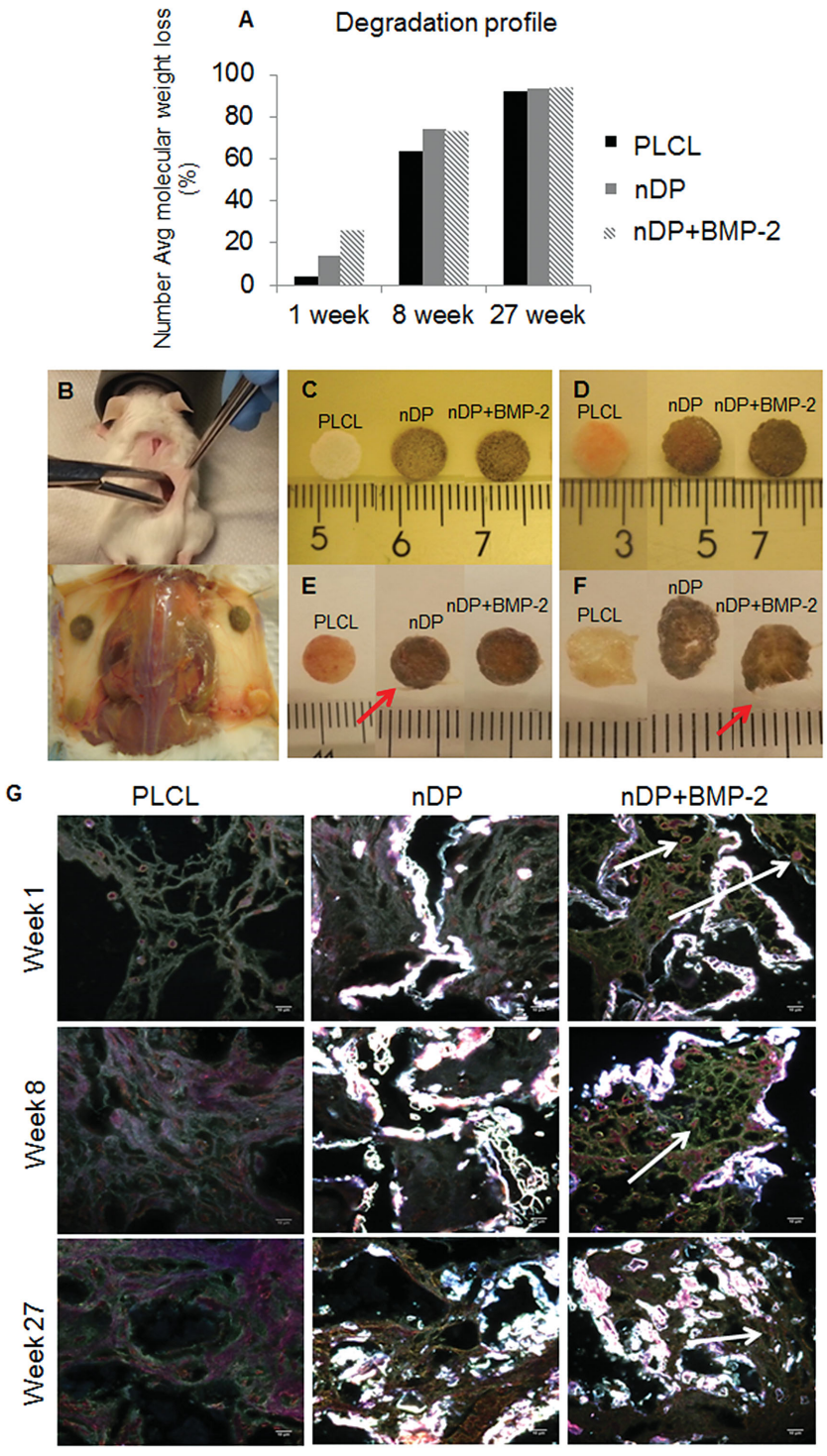

Figure 1. Implantation pattern, degradation behavior of implanted scaffolds and fate of incorporated nanodiamond particles. A) Molecular weight loss of the different scaffolds measured by SEC expressed in percentage depicting their degradation profile (average of two independent measurements). B) Subcutaneous implantation of four random scaffolds per animal. Macroscopic images of the scaffolds C) before implantation, D) 1 week postimplantation, E) 8 weeks postimplantation, F) 27 weeks postimplantation. A thin fibrous tissue coating on retrieved scaffolds is indicated by the red arrow. G) Images taken with Cytoviva showing the abundant presence of nDP in the implantation site even after 27 weeks. Magnification 1000×. Bright areas are the nanodiamonds. Pores are invaded with tissue ingrowth as seen in green color and the cell nuclei are observed as red dots (white arrows).

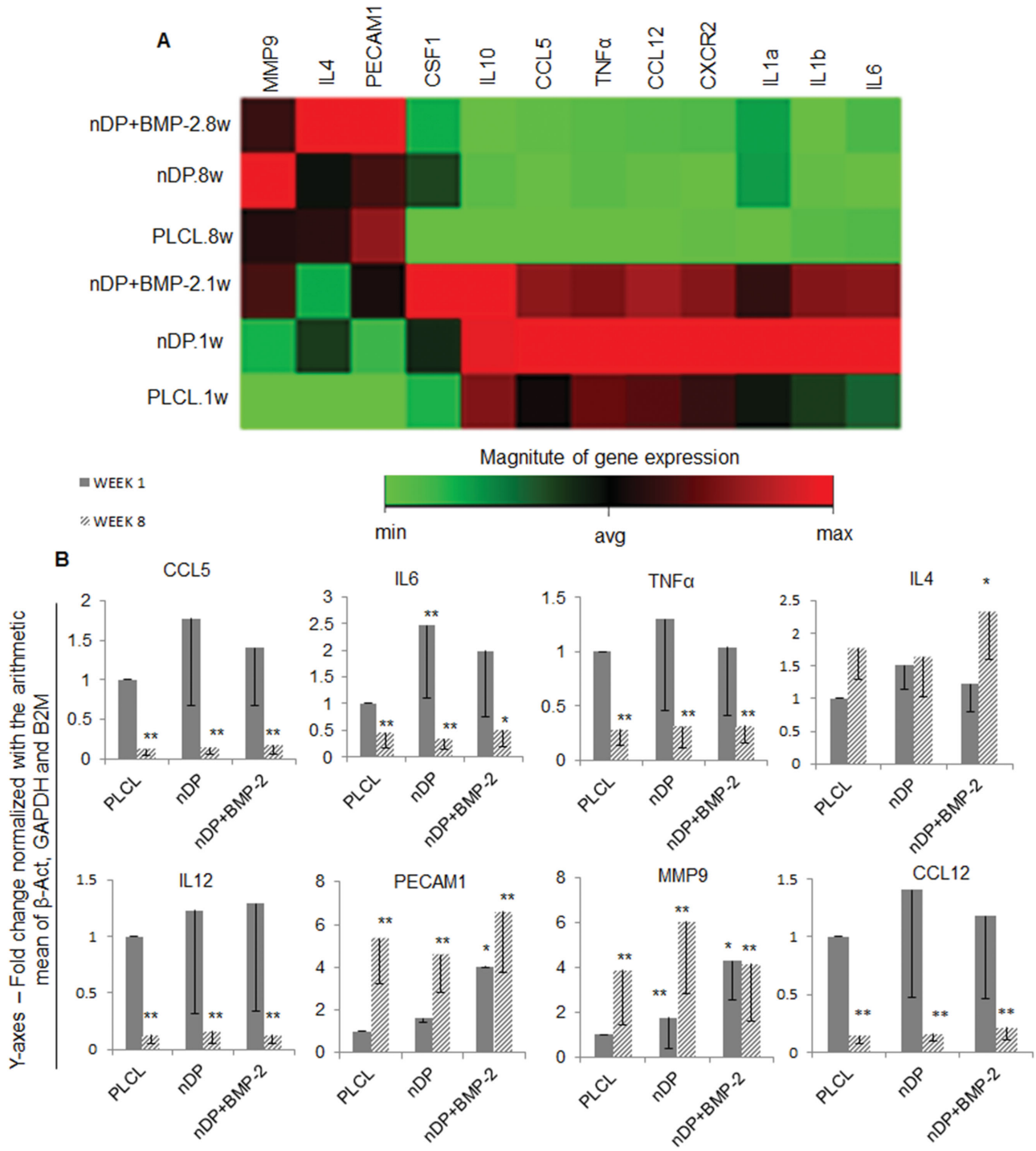

Figure 2. Inflammatory cytokine and chemokine expressions. A) Clustergram showing relative mRNA expression of preselected pro- and anti-inflammatory markers from the cells that infiltrated in the scaffolds at week 1 and 8. B) Some of the significantly expressed genes plotted as quantitative fold change in the y-axis. Data are expressed as $2^{-\Delta\Delta Ct}$ and 95% confidence interval relative to PLCL group at week 1. Values were normalized with the arithmetic mean of β-Act, GAPDH, and B2M. (* $p < 0.05$, ** $p < 0.001$.)

(IL4, MMP9, PECAM1) showed the reversed pattern, with upregulation at week 8 and the greatest expression from nDP or nDP+BMP-2 group.

Inflammatory activity was also estimated histologically by the host tissue response at weeks 1, 8, and 27. Representative sections (H&E staining) of the different scaffolds explanted at week 1 are presented in (**Figure 3**). The void spaces histologically observed between tissues and cells represent the cross sections of the scaffolds. At week 1 the connective tissue was loose, with thin collagen fibers and a thin layer of host cell

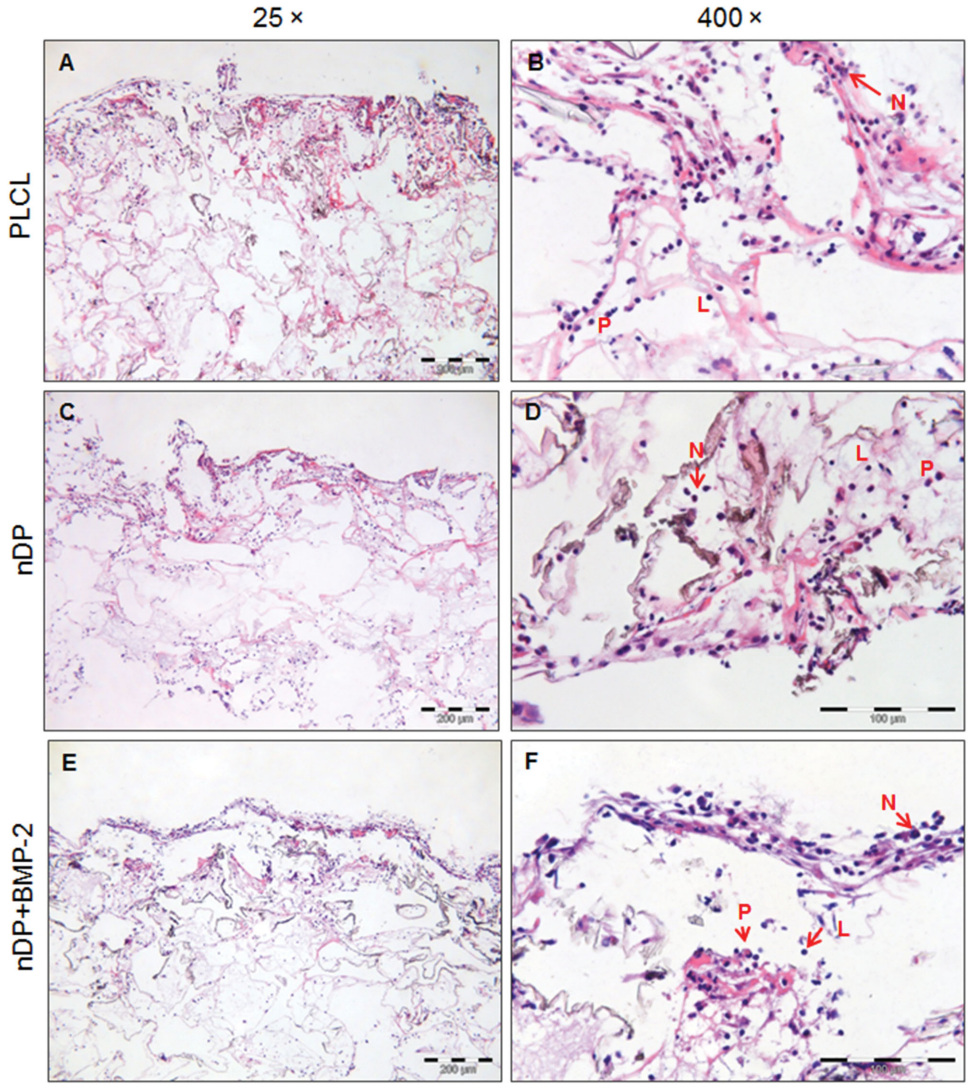

Figure 3. Inflammatory reaction of host tissue. Images of H&E stained sections at week 1 postimplantation. (A, C, and E) PLCL, nDP, nDP+BMP-2, respectively, show the inflammatory cell influx greatest at the periphery. Magnification 25×. Scale bar = 1 μm. (B, D, and F) PLCL, nDP, nDP+BMP-2, respectively, at 400× magnification show examples of the different scaffolds in the three groups at week 1 postimplantation showing the different inflammatory cells recruited. N – neutrophils, L – lymphocytes, P – plasma cells. Scale = 100 μm.

infiltration seen at the interface between host and scaffold. The inflammatory infiltrate consisted predominantly of neutrophils and lymphocytes at week 1, mainly at the periphery of the scaffold, diminishing toward the center of the scaffold (Figure 3A,C,E). The presence of acute inflammatory cells was more prominent in the PLCL scaffold group (neutrophils $p < 0.01$, plasma cells $p < 0.01$) than in the other groups (**Figure 4**). At week 8 the pores were mainly occupied by fibrous tissue containing fibroblasts. Inflammatory cells (lymphocytes and plasma cells) were still visible in the porous structure at week 8 after implantation; however, their presence reduced at 27 weeks. As the inflammatory response became chronic, cells appeared to be increased toward the inner porous structure of the scaffold. Multinucleated foreign body giant cells (FBGC) were not seen at week 1 in any of the groups. Their presence was observed at week 8 and increased with time, except in nDP+BMP-2 scaffolds, where fewer FBGC were seen at week 27 than at week 8 (Figure 4). PLCL scaffolds were observed to recruit higher numbers of FBGC than other scaffold groups and this corresponded with their molecular weight loss. The morphology of the FBGC was typical for a foreign body reaction, with irregular shape and more than 20 nuclei distributed randomly within their cytoplasm.

Degradation of scaffolds, as assessed microscopically on the histological sections, was observed as a loss of the regular appearance of the scaffold and its replacement by fibers. Remnants of scaffold material could be observed histologically at week 8 (**Figure 5**B 'S') predominantly at the center, indicating that the scaffolds degraded more at the periphery than at the center. FBGC were seen commonly very close to the remnants of the material (Figure 5 A–C, red arrows). No macroscopically detectable fibrous capsule was seen at week 1 in all scaffold

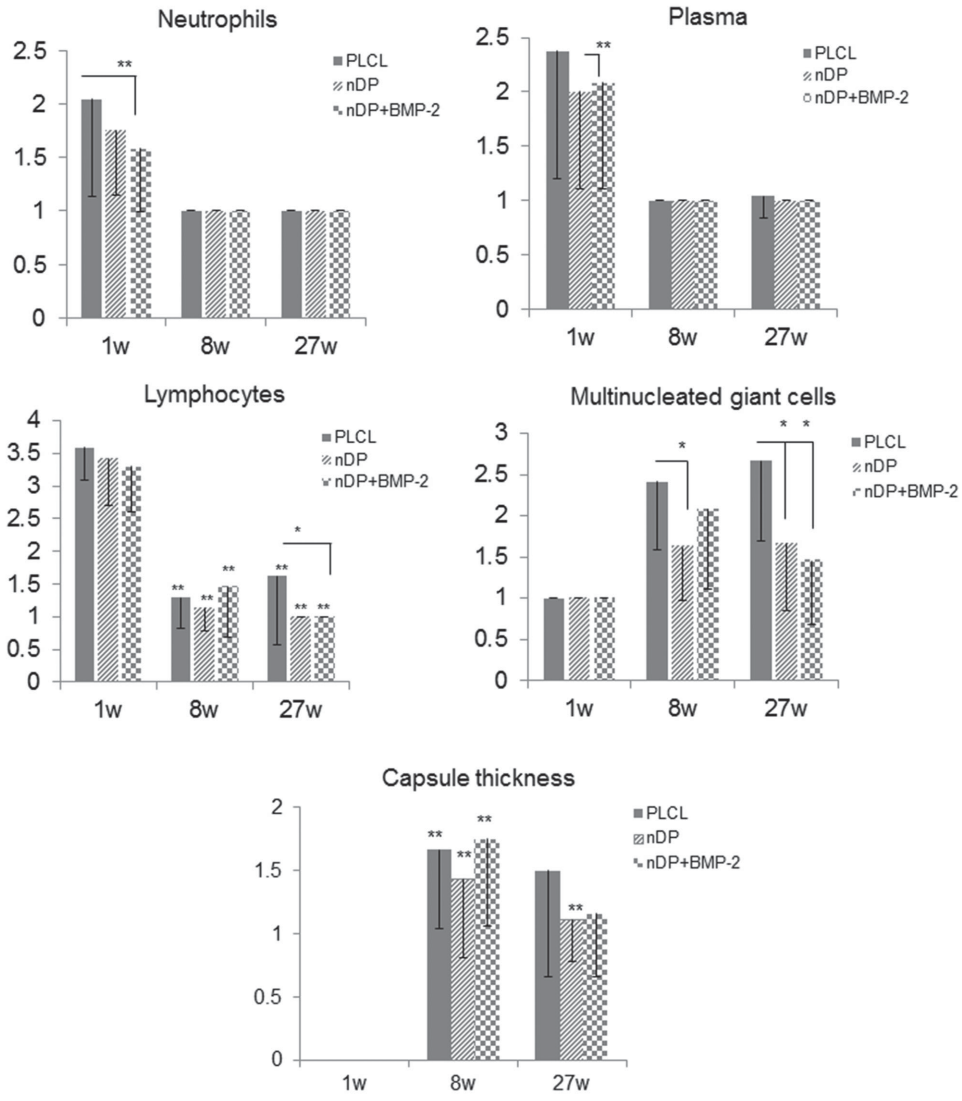

Figure 4. Histological grading of early and late inflammatory cells at weeks 1, 8, and 27 for the three different scaffold types. Average score in the y-axis and data expressed with SD. (* $p < 0.05$, ** $p < 0.001$.) Stars (*) without lines express significance between groups at different time points.

groups, but at week 8 and 27 after implantation, a very thin fibrous tissue surrounding the samples and strongly attached to them was observed (Figure 1E,F, red arrows). Generally, at week 8, the capsule was seen in all groups, with an average of less than nine concentric layers of fibroblasts observed microscopically (Figure 5D–F) and containing collagen fibers with few inflammatory cells. By week 27, the capsule was mostly fibrous and its thickness was reduced to less than four concentric fibroblast layers on average in all groups. The PLCL scaffold was surrounded by the thickest capsule (Figure 4).

3.3. Angiogenic and Ectopic Bone Stimulation

The osteogenic potential and angiogenic efficacy of the different scaffolds was evaluated at the molecular level by RT-PCR of selected markers significant for both (**Figure 6**A,B). Osteogenic potential of the scaffolds was further evaluated by ectopic bone formation/mineralization by micro-CT. mRNA of BMPR1A and RUNX2 were significantly upregulated in the nDP+BMP-2 scaffold group at week 1. MRNA levels of ALP ($p = 0.01$) also showed a pronounced upregulation at week 1 stimulated by BMP-2. At week 8 ALP downregulated in nDP-PHY scaffolds but continued to be highly expressed in other groups. Collage type 1 and type 2 markers (mRNA Col1a2 and Col2a1, respectively) also showed a similar trend of significant highest expression in nDP+BMP-2 followed by nDP at week 1 and week 8.

mRNA levels of angiogenesis markers were all seen to be significantly upregulated at week 8 in all groups. Generally, nDP and nDP+BMP-2 scaffolds were seen to have higher expressions compared to CL at week 1. nDP+BMP-2 showed a significant upregulation of ANGPT1 ($p = 0.03$) and FGF2 ($p = 0.003$) at week 1.

Subcutaneous implantation of the scaffolds lead to pronounced ectopic bone formation in nDP+BMP-2 scaffolds. A representative 3D reconstruction of nDP+BMP-2 scaffold

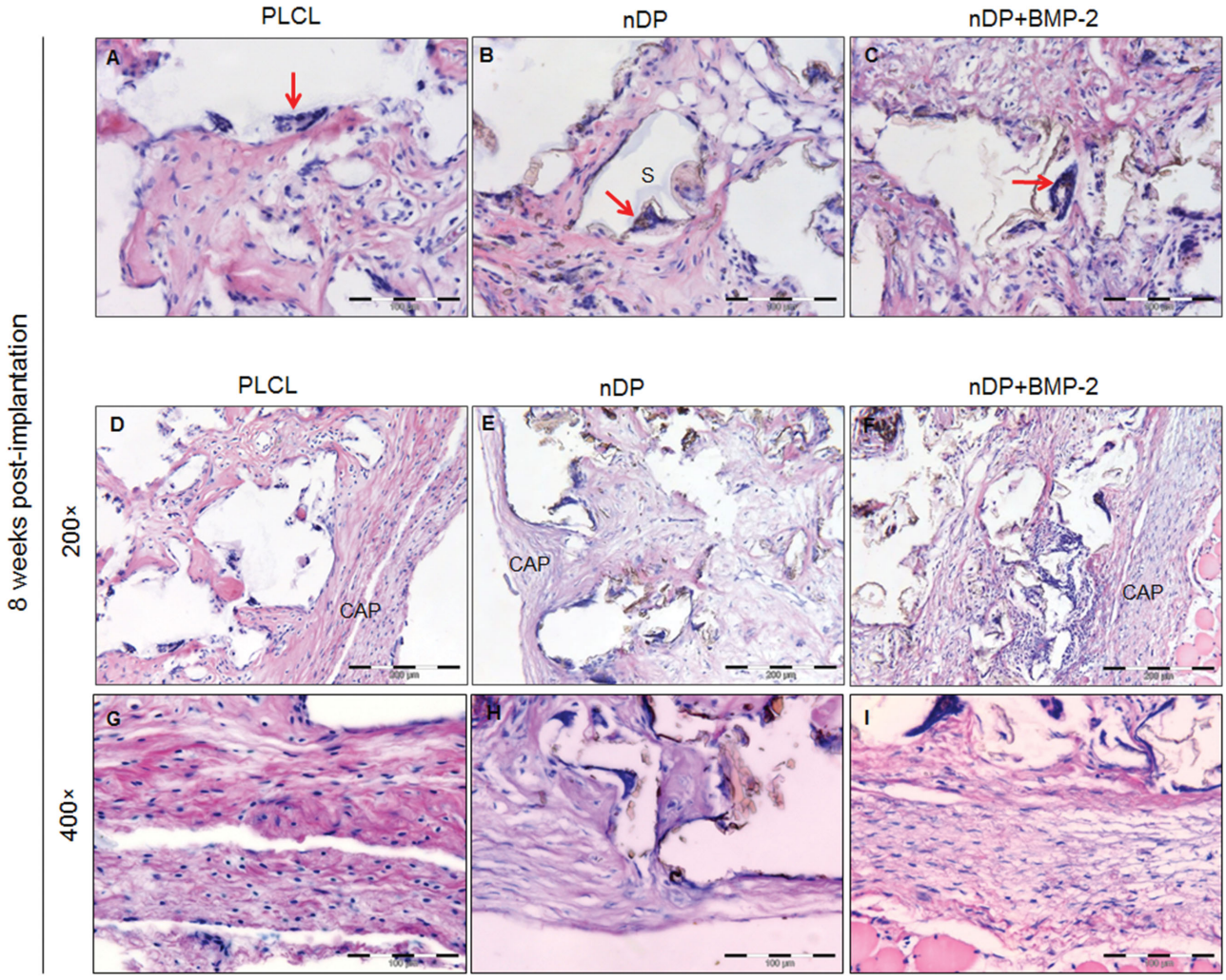

Figure 5. Light images of H&E stained scaffolds at week 8 postimplantation. A–C) PLCL, nDP, and nDP+BMP-2, respectively, showing the different foreign body giant cells (red arrows) and the remnant scaffold indicated "S," D–F) PLCL, nDP, and nDP+BMP-2, respectively, and show the varying thickness of the capsules "CAP" surrounding the different scaffolds at week 8. Magnification 200×. Scale bar = 200 μm. G–I) Magnification 400× of the different fibrous capsules. Scale bar = 100 μm.

scanned after 8 weeks postimplantation showing the mineralized tissue (Figure 6C,D).

4. Discussion

The biocompatibility of the polymeric scaffolds was evaluated utilizing a standard, previously established subcutaneous mouse model for determining tissue responses to biomaterials.[26] This in vivo model more closely reflects the natural situation than in vitro assessments.

The degradation profile of unmodified PLCL scaffolds has been evaluated previously.[26] In the current study, the explanted scaffolds were extracted with chloroform, and the polymeric residue was weighed and analyzed, thus demonstrating that the degradation of the scaffolds occurred by polymer chain cleavage, resulting in a reduction of molecular weight. These polyesters are known to degrade by hydrolysis. The nDP used to modify the scaffolds has been shown to increase the hydrophilicity of the scaffolds and hence improve cellular attachment and differentiation[11] due to the hydroxylated surfaces.[29] This also enhanced the absorption of water and thus accelerated the hydrolysis process causing the higher molecular weight loss from nDP and nDP+BMP-2 scaffolds relative to PLCL at week 1 and week 8. The degradation analyzed after week 1 is relatively fast, but may be the result of pre-existing water soluble low molecular weight oligomers created during sterilization being leached out without need for chain cleavage.[26] It was also observed that the increased water diffusion into the nDP modified scaffolds may have promoted a bulk pattern of erosion. In bulk erosion, the polymer chain scission occurs throughout the scaffold in the amorphous part of the polymer, thus although it does not change much in external dimensions, the molecular weight decreases early. This was seen in the macroscopic pictures (Figure 1) of the harvested scaffolds after 8 and 27 weeks where the nDP and nDP+BMP-2 scaffolds

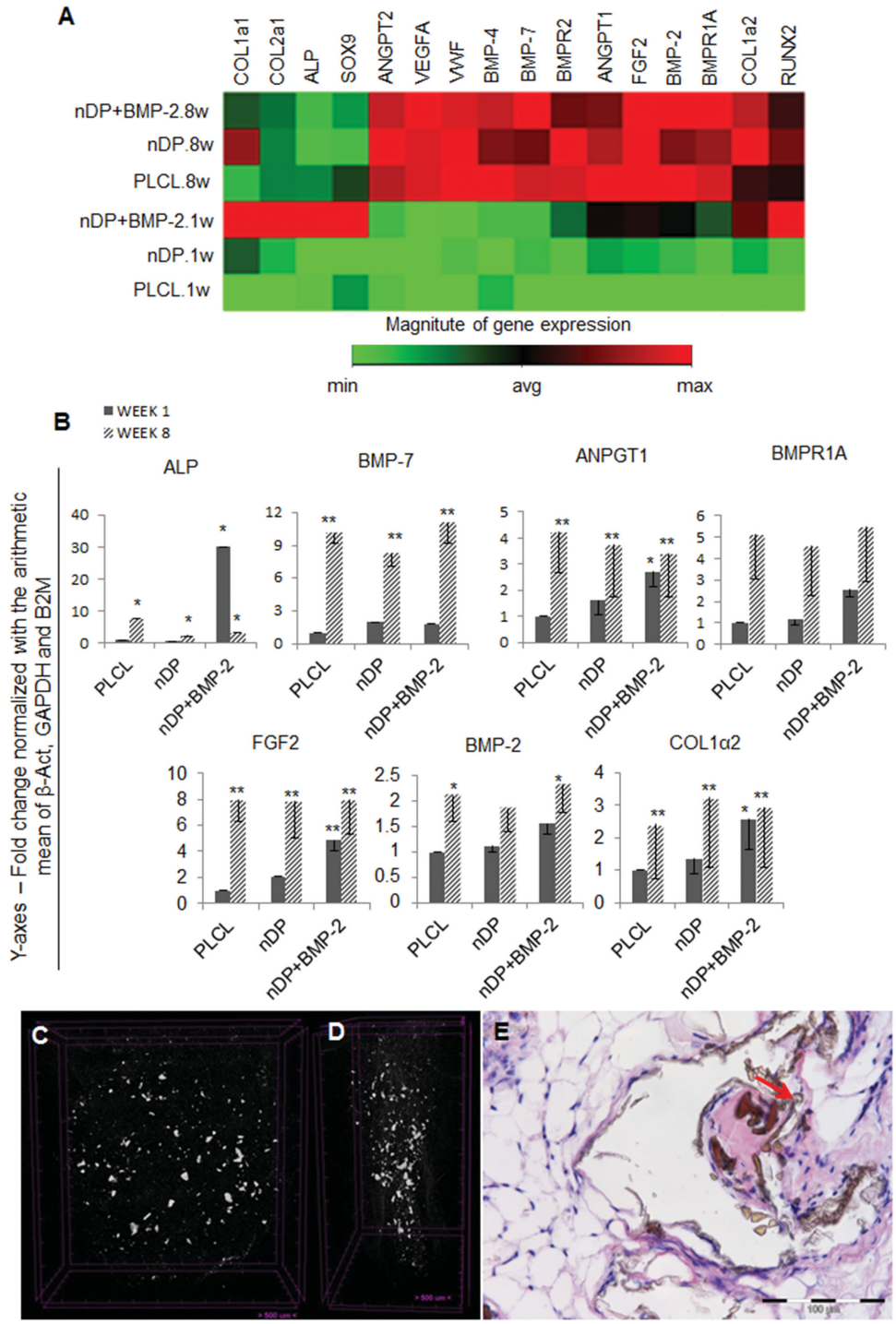

Figure 6. Osteogenic and angiogenic potential of the different scaffolds. A) Clustergram showing relative mRNA expression of preselected angiogenic and osteogenic markers from the cells infiltrating the scaffolds after week 1 and 8. B) Some representative significantly expressed genes plotted in a quantitative fold change in the y-axis. Data were expressed as $2^{-\Delta\Delta Ct}$ and 95% confidence interval relative to PLCL group at 1 week. Values were normalized with the arithmetic mean of β-Act, GAPDH and B2M. (* $p < 0.05$, ** $p < 0.001$.) C) Micro-CT 3D reconstructed image D) lateral image. E) Image with H&E staining, red arrow indicating mineralized area. Magnification 400×. Scale bar = 100 μm.

were physically present but showed considerably thinner and translucent areas in the centre. Tissue response also plays a role in in vivo degradation. The nDP modified scaffolds exerted an upregulated inflammatory response at the mRNA level at week 1 (Figure 2) relative to the PLCL scaffolds, suggesting the presence of the early stage reactive oxygen species, which has been reported to degrade polymers. The reactive oxygen species induce migration of inflammatory cells that can oxidize polymer

chains.[30] Previously, it was demonstrated that the PLCL scaffolds implanted in rat calvaria decrease their molecular weight by around 70% after 91 days.[26] Regarding these same unmodified scaffolds, our study showed in two months almost 60% of M_n is reduced. Hence comparable rate of degradation is seen although the implantation site and size of animal was different. An important aspect of the present study is that the evaluation was for up to 27 weeks (half a year), which is a long in vivo assessment for such studies. The present data showed that after 27 weeks all three scaffolds lost a comparable molecular weight of 90% of the original molecular weight. Interestingly, the nDP present in the scaffolds' implantation area at week 27 suggests that the particles stay in the tissue even after almost 90% of the scaffold has degraded without eliciting side effects. The decrease in the pH (acidic environment) during scaffold degradation leads to the agglomeration of the particles, which immobilizes them and prevents adverse effects commonly induced by nanoscale materials. The fast degradation might be considered an undesirable feature in theory, since previous studies have shown that the slower the degradation, the better the host response,[28] but in fact this was not seen in our study, probably attributed to nDP and BMP-2 modifications. Although the nDP and nDP+BMP-2 scaffolds that degraded faster had elevated mRNA levels of proinflammatory markers relative to PLCL at week 1, the inflammatory cells present histologically in the site, particularly chronic inflammation cells, were significantly less at the later time points.

Implanted materials, such as scaffolds, cause the body to initiate an inflammatory response. This inflammatory response is known as the foreign body reaction (FBR), which has three phases: onset, progression, and resolution.[31] The onset phase shares characteristics with wound healing after injury. In our study, implantation of the biomaterials induced tissue injury, which caused the release of inflammatory mediators including a wide range of cytokines. Although our study did not include a sham surgical or "injury" control, the initial inflammatory response between the scaffold groups differed, which is more likely to be related to the modifications than to the surgical injury.

The surface chemistry of an implanted scaffold strongly influences the composition of the adsorbed protein layer and the host response is induced indirectly by these protein layers.[31] Previous reports have shown that hydrophilic/neutral surfaces inhibit inflammatory cellular adhesion.[15] This explains the reduced number of inflammatory cells seen in the nDP modified scaffolds compared to PLCL scaffolds in this study. Hydrophilic surfaces were also shown to downregulate proinflammatory gene expression by macrophage-like cells in vitro.[32] The nDP modified scaffold groups demonstrated the highest mRNA expression levels of proinflammatory markers (CCL5, IL6, TNFα, and CCL12) at week 1 postimplant. These elevated levels of inflammatory cytokines from modified groups might be due to changes occurring in fibrinogen adsorption, as previous studies have shown that materials with hydroxyl group terminations might exhibit inflammatory reactions due to their effects on fibrinogen.[33] This reduced inflammatory cell count but high inflammatory marker expression in the modified groups can also be due to a negative feedback phenomenon, or posttranscriptional control, or increased levels produced by macrophages as a result of the faster degradation of nDP modified scaffolds relative to PLCL. Other studies also postulate that although the number of inflammatory cells is reduced in hydrophilic surfaces, but they are more activated thus releasing higher cytokine amounts.[15,34] However, the assessment of cytokines in vivo is challenging due to the local nature of their production and effects and the complex cellular interactions of a wide range of cytokines at any given time point.

The nDP+BMP-2 scaffolds carried BMP-2 and have previously been shown to sustain release of BMP-2 at low doses.[12] Since BMP-2 belongs to the TGF-β superfamily of proteins and TGF-β is known to have a dual role in inflammatory modulation, reducing TNFα production and promoting extracellular matrix production.[35] The sustained release of BMP-2 may explain the reduced levels of TNFα mRNA seen with nDP+BMP-2 scaffolds relative to nDP scaffolds. This result supports previous observations that slow BMP-2 release attenuated inflammation[36] and enhanced osteogenic potential. Another recent study also observed the expression of TNFα to be increased in a nonmodified collagen-chitosan scaffold compared to a modified version delivering growth factors from chitosan nanoparticles.[37] Alternatively, it is also possible that the functional terminals in nDP are occupied with the bound BMP-2, thus preventing the nDP from influencing host tissue responses.

The tissue samples were cut in half before being embedded; hence all the sections were produced from the same location for standardized histological evaluation. Neutrophils are the first line of defense in an inflammatory reaction,[31] and they were seen in all scaffold groups, suggesting that the host response was in an early/acute inflammatory stage during the first week. However, a significant increase in neutrophils was seen in the PLCL scaffolds at week 1 relative to the other scaffolds. This may be related to the surface properties of the different scaffolds and the initial variations in protein adsorption with subsequent effects on cell activation, recruitment and adherence. Polymers with increased hydrophobicity have been revealed to increase inflammatory cells' (monocytes) attachment.[38] PLCL scaffold being relatively hydrophobic (around 80°, measured by water contact angle),[39] these scaffolds would also have greater affinity for body fluid proteins than the modified scaffolds, which might lead to conformational changes in the proteins due to the hydrophobic interactions that are thought to be responsible for recruiting inflammatory cells and causing a pronounced foreign body reaction.[31,40] After week 8, the majority of cells seen in all specimens were mononuclear and giant cells, representing the typical foreign body response to biomaterials. The formation of FBGC is through the fusion of macrophages adherent to the implanted scaffold. The number of FBGC formed is related to degradation material.[19] The greatest number of FBGC was seen in the PLCL scaffolds at week 8, consistent with that this group being the least degraded scaffold at that time point and thus having more material available to be degraded. Although the nDP+BMP-2 had the next greatest score for FBGC at week 8, it was the fastest to degrade compared to other groups. This can be attributed to the upregulated IL4 mRNA levels of for that group at week 8, which has been reported to directly induce formation of FBGC.[41]

The morphology of FBGC was different between the scaffold groups. Phenotypic differences in FBGC have been reported to occur as a result of material surface properties,[41] thus the surface created by the nDP and their agglomerates may induce the cells to flatten in order to come in better contact with the material.

Upregulation of the tissue regeneration/healing markers IL4 and MMP-9 at week 8, when proinflammatory markers were decreasing is predictable as the phases of inflammation progress. MMP-9 has been associated with modulation of inflammation by extracellular remodeling and signaling during a foreign body reaction.[42] Emerging evidence suggests the active participation of MMP-9 in clearance of inflammatory cells[43] and this is reflected here in the decrease in lymphocytes in the nDP scaffolds at week 8 and week 27 compared to the other scaffolds groups.

Although a capsule was seen surrounding the scaffolds histologically, it was not always complete in every section, therefore it was evaluated when found. The consistent presence of BMP-2 in the vicinity of the nDP+BMP-2 may play a role in the thick encapsulation around that group at week 8. However, the fact that the capsule was significantly reduced in thickness by week 27 in the nDP and nDP+BMP-2 groups when seen suggests improved biocompatibility of these scaffolds and is an expected phenomenon with osteogenecity.[44] The bioactivity of physisorped BMP-2 was also demonstrated by upregulation of BMPR1A and RUNX2 by week 1, indicating activation of the BMP signaling pathway and a subsequent increase of osteogenicity.[45] This led to increased mRNA expression for ALP and BMP-2 in the nDP+BMP-2 scaffolds. The significantly elevated levels of COL1a2 and COL2a1 at week 1 in nDP+BMP-2 scaffold group demonstrate the presence of early osteogenic potential before mineralization. Thus, the elevated inflammatory response at week 1 from the nDP modified scaffolds can also be considered as the inflammatory response prior to the regeneration process. In further support of this, micro-CT analysis revealed mineralization as nodules-like spreading within the nDP+BMP-2 scaffolds at week 8. Histologically, these sites of mineralization were confirmed as a mineralization or hyalinised cartilage. This supports previous reports from our lab demonstrating that this mode of binding BMP-2 to scaffold and delivery of a very low amount encouraged early bone formation in a critical size rat mandible defect.[12,46] The subcutaneous area is relatively lacking in circulation[47] and tissue regeneration after scaffold implantation can therefore be a challenge. Despite this, modification with nDP resulted in a significant increase in angiogenic markers seen by week 1. In addition, a decrease in inflammation as reflected by a reduction in inflammatory cells at week 8 was seen.

In conclusion, the results presented here demonstrate that modifying poly[(L-lactide)-co-(ε-caprolactone)] scaffolds with nDP does not aggravate the tissue response in a subcutaneous implantation model and that this mode of physisorbed BMP-2 delivery shows attenuation of inflammatory responses. The identification of functional groups in nDP that can be tailored to control protein adsorption and subsequent host response is warranted and can be of major value to the field of tissue engineering. In a clinical setting, nDP functionalized copolymer scaffolds with or without physisorbed BMP-2 would thus afford a means of reducing inflammatory activity and of dramatically lowering the pharmacological dose of the osteogenic agent to a safe and economically feasible level.

Supporting Information

Supporting Information is available from the Wiley Online Library or from the author.

Acknowledgements

The research leading to these results has received funding by the European Union's Seventh Framework Programme under grant agreement number 242175-VascuBone and Helse Vest project no 911902 (D.E.C.). The authors thank Mr. Bendik Nordanger, Department of Pathology, Haukeland University Hospital, Bergen, Mrs. Siren Hammer Østvold, Dr. Mohamed Ibrahim, and Dr. Mohammed Yassin, University of Bergen, for technical assistance. The authors thank Dr. Michele Cottler-Fox, University of Arkansas for Medical Sciences, Little Rock, USA for English revision and constructive criticism of the manuscript.

Received: September 8, 2015
Revised: October 30, 2015
Published online: February 8, 2016

[1] F. J. O'Brien, *Mater. Today* **2011**, *14*, 88.
[2] W. G. De Long, T. A. Einhorn, K. Koval, M. McKee, W. Smith, R. Sanders, T. Watson, *J. Bone Jt. Surg., Am. Vol.* **2007**, *89A*, 649.
[3] E. S. Place, J. H. George, C. K. Williams, M. M. Stevens, *Chem. Soc. Rev.* **2009**, *38*, 1139.
[4] S. B. Idris, S. Danmark, A. Finne-Wistrand, K. Arvidson, A. C. Albertsson, A. I. Bolstad, K. Mustafa, *J. Bioact. Compat. Polym.* **2010**, *25*, 567.
[5] S. Danmark, A. Finne-Wistrand, M. Wendel, K. Arvidson, A. C. Albertsson, K. Mustafa, *J. Bioact. Compat. Polym.* **2010**, *25*, 207.
[6] K. Odelius, P. Plikk, A. C. Albertsson, *Biomacromolecules* **2005**, *6*, 2718.
[7] F. Khan, R. S. Tare, J. M. Kanczler, R. O. Oreffo, M. Bradley, *Biomaterials* **2010**, *31*, 2216.
[8] J. O. Smith, E. R. Tayton, F. Khan, A. Aarvold, R. B. Cook, A. Goodship, M. Bradley, R. O. Oreffo, *J. Tissue Eng. Regen. Med.* **2015**, DOI: 10.1002/term.2007.
[9] a) H. Hosseinkhani, M. Hosseinkhani, A. Khademhosseini, H. Kobayashi, *J. Controlled Release* **2007**, *117*, 380; b) T. Lou, X. Wang, G. Song, *Int. J. Biol. Macromol.* **2013**, *61*, 353; c) D. X. Wang, Y. He, L. Bi, Z. H. Qu, J. W. Zou, Z. Pan, J. J. Fan, L. Chen, X. Dong, X. N. Liu, G. X. Pei, J. D. Ding, *Int. J. Nanomed.* **2013**, *8*, 1855.
[10] a) V. N. Mochalin, O. Shenderova, D. Ho, Y. Gogotsi, *Nat. Nanotechnol.* **2012**, *7*, 11; b) Q. W. Zhang, V. N. Mochalin, I. Neitzel, I. Y. Knoke, J. J. Han, C. A. Klug, J. G. Zhou, P. I. Lelkes, Y. Gogotsi, *Biomaterials* **2011**, *32*, 87.
[11] Z. Xing, T. O. Pedersen, X. J. Wu, Y. Xue, Y. Sun, A. Finne-Wistrand, F. R. Kloss, T. Waag, A. Krueger, D. Steinmuller-Nethl, K. Mustafa, *Tissue Eng., Part A* **2013**, *19*, 1783.
[12] S. Suliman, Z. Xing, X. Wu, Y. Xue, T. O. Pedersen, Y. Sun, A. P. Doskeland, J. Nickel, T. Waag, H. Lygre, A. Finne-Wistrand, D. Steinmuller-Nethl, A. Krueger, K. Mustafa, *J. Controlled Release* **2015**, *197*, 148.
[13] E. J. Carragee, E. L. Hurwitz, B. K. Weiner, *Spine J.* **2011**, *11*, 471.

[14] D. T. Luttikhuizen, M. C. Harmsen, M. J. Van Luyn, *Tissue Eng.* **2006**, *12*, 1955.
[15] J. A. Jones, D. T. Chang, H. Meyerson, E. Colton, I. K. Kwon, T. Matsuda, J. M. Anderson, *J. Biomed. Mater. Res., Part A* **2007**, *83A*, 585.
[16] H. Liu, E. B. Slamovich, T. J. Webster, *Int. J. Nanomed.* **2006**, *1*, 541.
[17] S. J. Xie, Q. Zhu, B. Wang, H. J. Gu, W. Liu, L. Cui, L. A. Cen, Y. L. Cao, *Biomaterials* **2010**, *31*, 5100.
[18] A. S. Yazdi, G. Guarda, N. Riteau, S. K. Drexler, A. Tardivel, I. Couillin, J. Tschopp, *Proc. Natl. Acad. Sci. USA* **2010**, *107*, 19449.
[19] D. F. Williams, *Biomaterials* **2008**, *29*, 2941.
[20] K. Schmidt-Bleek, H. Schell, N. Schulz, P. Hoff, C. Perka, F. Buttgereit, H. D. Volk, J. Lienau, G. N. Duda, *Cell Tissue Res.* **2012**, *347*, 567.
[21] A. W. Ritting, E. W. Weber, M. C. Lee, *J. Hand Surg., Am. Vol.* **2012**, *37A*, 316.
[22] a) P. M. Mountziaris, P. P. Spicer, F. K. Kasper, A. G. Mikos, *Tissue Eng., Part B* **2011**, *17*, 393; b) Q. S. Wang, Y. L. Cui, L. N. Gao, Y. Guo, R. X. Li, X. Z. Zhang, *J. Biomed. Mater. Res., Part A* **2014**, *102*, 4098.
[23] a) A. Chatterjea, J. van der Stok, C. B. Danoux, H. P. Yuan, P. Habibovic, C. A. van Blitterswijk, H. Weinans, J. de Boer, *J. Biomed. Mater. Res., Part A* **2014**, *102*, 1399; b) J. Ratanavaraporn, H. Furuya, Y. Tabata, *Biomaterials* **2012**, *33*, 304.
[24] D. F. Williams, *Tissue Eng., Part A* **2014**, *20*, 1129.
[25] D. F. Williams, *J. Mater. Sci.-Mater. Med.* **2015**, 26.
[26] S. Danmark, A. Finne-Wistrand, K. Schander, M. Hakkarainen, K. Arvidson, K. Mustafa, A. C. Albertsson, *Acta Biomater.* **2011**, *7*, 2035.
[27] A. Kruger, F. Kataoka, M. Ozawa, T. Fujino, Y. Suzuki, A. E. Aleksenskii, A. Y. Vul, E. Osawa, *Carbon* **2005**, *43*, 1722.
[28] W. Ji, F. Yang, H. Seyednejad, Z. Chen, W. E. Hennink, J. M. Anderson, J. van den Beucken, J. A. Jansen, *Biomaterials* **2012**, *33*, 6604.
[29] A. Krueger, *Chemistry* **2008**, *14*, 1382.
[30] K. V. Brown, B. Li, T. Guda, D. S. Perrien, S. A. Guelcher, J. C. Wenke, *Tissue Eng., Part A* **2011**, *17*, 1735.
[31] J. M. Anderson, A. Rodriguez, D. T. Chang, *Semin. Immunol.* **2008**, *20*, 86.
[32] S. Hamlet, M. Alfarsi, R. George, S. Ivanovski, *Clin. Oral Implants Res.* **2012**, *23*, 584.
[33] K. M. Evans-Nguyen, L. R. Tolles, O. V. Gorkun, S. T. Lord, M. H. Schoenfisch, *Biochemistry* **2005**, *44*, 15561.
[34] J. M. Anderson, J. A. Jones, *Biomaterials* **2007**, *28*, 5114.
[35] D. P. Gong, W. Shi, S. J. Yi, H. Chen, J. Groffen, N. Heisterkamp, *BMC Immunol.* **2012**, *13*, 10.
[36] a) S. E. Kim, S. H. Song, Y. P. Yun, B. J. Choi, I. K. Kwon, M. S. Bae, H. J. Moon, Y. D. Kwon, *Biomaterials* **2011**, *32*, 366; b) G. Wu, Y. Liu, T. Iizuka, E. B. Hunziker, *Biomaterials* **2010**, *31*, 7485.
[37] A. M. Rajam, P. Jithendra, A. B. Mandal, C. Rose, *J. Biomed. Nanotechnol.* **2014**, *10*, 508.
[38] W. G. Brodbeck, Y. Nakayama, T. Matsuda, E. Colton, N. P. Ziats, J. M. Anderson, *Cytokine* **2002**, *18*, 311.
[39] Y. Sun, Z. Xing, Y. Xue, K. Mustafa, A. Finne-Wistrand, A. C. Albertsson, *Biomacromolecules* **2014**, *15*, 1259.
[40] a) A. Hezi-Yamit, C. Sullivan, J. Wong, L. David, M. F. Chen, P. W. Cheng, D. Shumaker, J. N. Wilcox, K. Udipi, *J. Biomed. Mater. Res., Part A* **2009**, *90A*, 133; b) M. D. Swartzlander, C. A. Barnes, A. K. Blakney, J. L. Kaar, T. R. Kyriakides, S. J. Bryant, *Biomaterials* **2015**, *41*, 26.
[41] A. K. McNally, J. M. Anderson, *J. Biomed. Mater. Res., Part A* **2015**, *103*, 1380.
[42] S. MacLauchlan, E. A. Skokos, N. Meznarich, D. H. Zhu, S. Raoof, J. M. Shipley, R. M. Senior, P. Bornstein, T. R. Kyriakides, *J. Leukocyte Biol.* **2009**, *85*, 617.
[43] K. J. Greenlee, D. B. Corry, D. A. Engler, R. K. Matsunami, P. Tessier, R. G. Cook, Z. Werb, F. Kheradmand, *J. Immunol.* **2006**, *177*, 7312.
[44] G. Wu, E. B. Hunziker, Y. Zheng, D. Wismeijer, Y. Liu, *Bone* **2011**, *49*, 1323.
[45] T. D. Mueller, J. Nickel, *FEBS Lett.* **2012**, *586*, 1846.
[46] F. R. Kloss, R. Gassner, J. Preiner, A. Ebner, K. Larsson, O. Hachl, T. Tuli, M. Rasse, D. Moser, K. Laimer, E. A. Nickel, G. Laschober, R. Brunauer, G. Klima, P. Hinterdorfer, D. Steinmuller-Nethl, G. Lepperdinger, *Biomaterials* **2008**, *29*, 2433.
[47] M. A. Scott, B. Levi, A. Askarinam, A. Nguyen, T. Rackohn, K. Ting, C. Soo, A. W. James, *Stem Cells Dev.* **2012**, *21*, 655.